Wind Engineering Joint Usage/Research Center
FY2025 Research Result Report

Research Field: Wind-Hazard Mitigation・Wind-Resistant Construction field
Research Year: FY2025
Research Number: 25252006
Research Theme: Aerodynamic characteristics of a tree model based on wind tunnel test and FSI simulation

Representative Researcher: Jingxue Wang

Budget [FY2025]: 300,000 JPY

1. Research Aim

Trees play a crucial role in reducing wind speed, improving the microclimate, and providing numerous ecological benefits, among other functions. Wind is the major mechanical excitation for trees. Research indicates that, with ongoing climate change, the damage to trees caused by strong winds is gradually increasing. Understanding the wind effects on trees and how their crown features influence the corresponding effects is essential for estimating potential damage.

The objective of this study is to investigate the aerodynamic characteristics of a tree model based on wind tunnel test and fluid-structure interaction (FSI) simulation. The aerodynamic wind loading and wind-induced responses of the tree are examined comprehensively. The findings provide fundamental insights into the wind-induced stability of trees under extreme wind conditions.

2. Research Method

2.1 High-Frequency Force Balance Test

The experiment was conducted in the turbulent boundary layer wind tunnel in TPU. The wind tunnel has the test section of 19 m in length, 2.2 m in width, and 1.8 m in height. The wind speed is adjustable in the range of 0.5 to 15m/s. According to a geometric scale ratio of 1:20, a scaled *Pinus sylvestris* var. *mongolica* tree model with a height of 50 cm was fabricated. To reduce additional inertial effects caused by the self-weight of the model under fluctuating wind loads, lightweight materials were adopted. The trunk and branches were made of high-strength aluminum rods with a circular cross-section of 1 mm in diameter (density ρ = 2700 kg/m^3, elastic modulus E = 6.91 × 10^1 Pa), which were welded into a spatial framework to form the bare trunk model without a crown, as shown in Figure 1(a). On this basis, three typical crown configurations were constructed to systematically investigate the influence of crown morphology on aerodynamic characteristics. A crown skeleton was 3D-printed from nylon (same density as above) and internally partitioned into

six compartments. This skeleton was assembled with the bare trunk to produce a skeleton-type crown model (Figure 1(b)), which features a high porosity and represents a sparse crown. A lightweight nylon mesh was then wrapped over the skeleton to form a film-covered crown model (Figure 1(c)), reducing the crown porosity through a continuous surface and thereby mimicking a dense crown. Finally, the skeleton was filled with raffia grass to create a porous-filled crown model (Figure 1(d)). This model maintains a certain permeability while enhancing the flow-blocking effect, and is used to simulate the complex porous-media flow characteristics inside the tree crown.

(a) Bare trunk (without canopy)

(b) Skeleton canopy

(c) Film-covered canopy

(d) Raffia-filled canopy

Figure 1 Scaled tree model for wind tunnel test

A grid rectification device, illustrated in Figure 2, was placed at the entrance of the test section. It consisted of wooden bars measuring 115 mm in width and 20 mm in thickness. The bars are arranged in a 4-row by 5-column array with a spacing of 385 mm between adjacent bars. The grid was positioned 3m upstream of the model to break up large-scale eddies and induce small-scale homogeneous turbulence in its wake, thereby generating a uniform turbulent field that meets the test requirements in the model region.

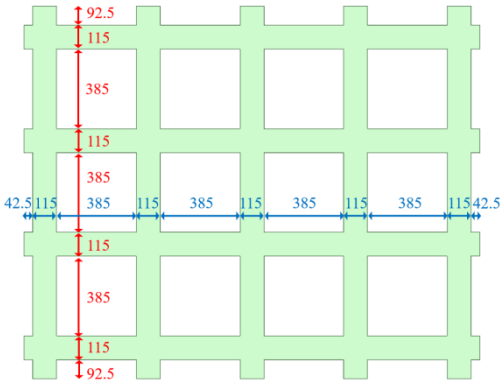

Figure 2 Schematic diagram of the grid rectification device for wind tunnel test

The wind profile was measured using a hot-wire anemometer. The fan rotational speed was set to 500r/min, the sampling duration per point was 60s, and the sampling frequency was 1000Hz. The distributions of the mean wind speed and turbulence intensity at the model location are shown in Figure 3. Owing to the spacer between the force balance and the tree model, the top of the model corresponded to a height of approximately 535 mm, where the turbulence intensity stabilized at around 15% and the mean wind speed fell within a gradient-free uniform region. Four inflow conditions were generated by the wind tunnel fan, resulting in wind speeds of 2.64 m/s, 4.21 m/s, 5.77 m/s, and 7.39 m/s measured at the tree model top height, in order to investigate the mean and fluctuating aerodynamic force responses under different inflow intensities and crown configurations. A velocity scale ratio of 1:8 was adopted, which yielded a time scale ratio of 1:2.5 combined with the geometric scale ratio of 1:20. The sampling frequency was set to 400 Hz to ensure sufficient accuracy for higher-order statistics and power spectral analysis. The sampling duration for each test case was set to 2400 s, which was equivalent to 6000 s in full scale, corresponding to ten standard 10 minutes observation samples.

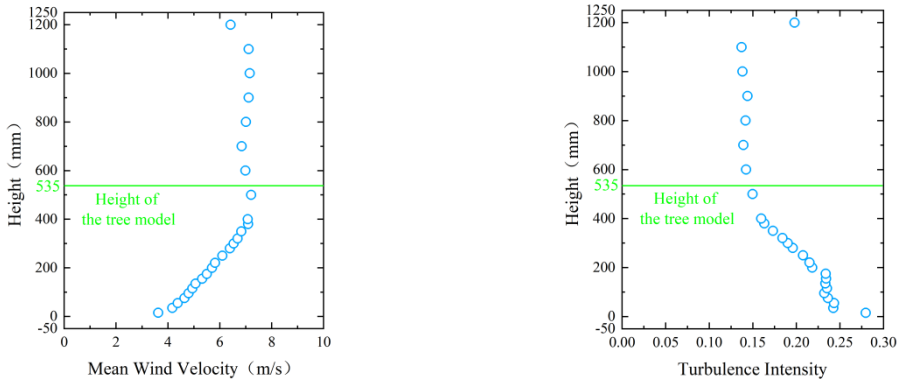

(a) Mean wind speed (b) Turbulence intensity

Figure 3 Incoming flow field characteristics for wind tunnel test

2.2 Fluid-Structure Interaction (FSI) simulation

In this study, one-way and two-way fluid-structure interaction (FSI) simulations were employed to evaluate the influence of aeroelastic effects on the wind-induced response of

trees. The numerical simulations were performed on the Ansys Workbench platform, using the Geometry, Fluent, Transient Structural, and System Coupling modules to establish a two-way tree-flow field coupling model. In the fluid domain, Fluent solved the wind field around the tree and output the transient pressure and wall shear stress on the tree surface, which were transferred to the structural domain as aerodynamic loads. In the structural domain, Transient Structural computed the vibration and deformation response of the tree at the current time step, and the resulting structural displacements were fed back to the fluid domain through System Coupling.

A uniform inflow condition was imposed at the inlet, with a wind speed of 30 m/s. The bottom surface of the computational domain and the tree surface were set as no-slip walls; the top and two sides adopted symmetry boundary conditions; and the outlet was set as a free outflow. The k-ω SST turbulence model was selected, as it combines the near-wall advantage of the k-ω model with the far-field stability of the k–ε model, capable of automatically switching between wall functions and direct resolution, and is suitable for capturing the flow characteristics of most complex conditions. An explicit mesh update method was employed for the dynamic mesh, integrating spring smoothing, remeshing, and dynamic layering to handle mesh distortion caused by boundary motion. For data transfer, a profile-preserving mapping algorithm was used for spatial interpolation to balance flux conservation and the preservation of data distribution features. A fixed time-step strategy was adopted for temporal coordination; the fluid and structural solvers advanced alternately in a strictly synchronous manner, and the coupling solver performed implicit strong coupling iterations.

3. Research Result

3.1 Aerodynamic Characteristics from Wind Tunnel Tests

To facilitate a comparison of the aerodynamic characteristics of the tree models under different wind speeds, the six mean aerodynamic force coefficients were statistically analyzed for the four models under all four wind speed conditions: drag coefficient $\overline{C_D}$, lift coefficient $\overline{C_L}$, lateral force coefficient $\overline{C_Z}$, and the moment coefficients about the cross-wind, along-wind, and vertical axes C_{ML}, C_{MD}, and C_{MZ}. The results are listed in Table 1 to Table 4, respectively.

Overall, the aerodynamic force coefficients of the bare trunk model, the skeleton-type crown model, and the film-covered crown model exhibited relatively small variations across the tested wind speed range, indicating good stability. The overall trend of the porous-filled crown model remained broadly consistent with the above three models; however, under the lowest wind speed of 2.64 m/s, some coefficients deviated to a certain extent, suggesting that the test results of this model at low wind speeds are more sensitive to inflow fluctuations and measurement errors. Moreover, to more accurately reflect the actual

loading state of the bare trunk model, supplementary aerodynamic coefficients calculated using the frontal area of the trunk and branches as the reference area are also provided. In terms of magnitude, the along-wind force coefficient $\overline{C_D}$ and the cross-wind bending moment coefficient $\overline{C_{ML}}$ are the dominant aerodynamic response components, showing relatively regular trends across different models and wind speeds. In contrast, $\overline{C_L}$, $\overline{C_Z}$, $\overline{C_{MD}}$, and $\overline{C_{MZ}}$ values are generally small, with some results fluctuating around zero and exhibiting less pronounced regularity.

Table 1 Mean aerodynamic force coefficients of bare trunk model (without canopy)

Wind speed (m/s)	$\overline{C_D}$	$\overline{C_L}$	$\overline{C_Z}$	$\overline{C_{MD}}$	$\overline{C_{ML}}$	$\overline{C_{MZ}}$
	A_c, A_b	A_c, A_b	A_c, A_b	A_c, A_b	A_c, A_b	A_c, A_b
7.39	0.88, 0.13	-0.02, 0.00	0.00, 0.00	0.00, 0.00	0.45, 0.07	-0.00, 0.00
5.77	0.87, 0.13	-0.04, 0.01	-0.05, 0.02	-0.00, 0.00	0.47, 0.07	0.01, 0.00
4.21	0.86, 0.12	-0.10, 0.01	0.02, 0.00	-0.02, 0.00	0.52, 0.07	0.03, 0.00
2.64	0.74, 0.11	-0.15, 0.05	0.03, 0.00	-0.05, -0.01	0.68, 0.10	0.11, 0.02

Table 2 Mean aerodynamic force coefficients of the skeleton-type crown model

Wind speed (m/s)	$\overline{C_D}$	$\overline{C_L}$	$\overline{C_Z}$	$\overline{C_{MD}}$	$\overline{C_{ML}}$	$\overline{C_{MZ}}$
7.39	0.86	-0.00	-0.04	0.00	0.49	-0.00
5.77	0.87	-0.01	-0.05	0.00	0.51	-0.00
4.21	0.89	-0.02	-0.06	-0.00	0.54	-0.00
2.64	0.87	-0.06	-0.09	-0.02	0.60	0.01

Table 3 Mean aerodynamic force coefficients of the film-covered crown model

Wind speed (m/s)	$\overline{C_D}$	$\overline{C_L}$	$\overline{C_Z}$	$\overline{C_{MD}}$	$\overline{C_{ML}}$	$\overline{C_{MZ}}$
7.39	1.03	-0.00	-0.06	-0.00	0.56	-0.01
5.77	1.03	-0.00	-0.07	-0.00	0.56	-0.01
4.21	1.04	0.01	-0.09	0.00	0.57	-0.01
2.64	1.04	0.02	-0.12	0.00	0.57	-0.01

Table 4 Mean aerodynamic force coefficients of the porous-filled crown model

Wind speed (m/s)	$\overline{C_D}$	$\overline{C_L}$	$\overline{C_Z}$	$\overline{C_{MD}}$	$\overline{C_{ML}}$	$\overline{C_{MZ}}$
7.39	1.15	0.01	-0.10	-0.01	0.64	-0.01
5.77	1.16	0.02	-0.04	-0.01	0.65	-0.01
4.21	1.17	0.03	0.07	-0.02	0.65	-0.00
2.64	1.21	0.03	0.30	-0.02	0.68	-0.00

Figure 4 presents the mean drag coefficient $\overline{C_D}$, mean lift coefficient $\overline{C_L}$, mean moment coefficient $\overline{C_L}$, and the corresponding fluctuating components C'_D, C'_L, and C'_{MD} for the four tree models under the 7.39 m/s condition. In terms of mean values, both $\overline{C_D}$ and $\overline{C_{ML}}$ increase monotonically as the crown transitions from absent to present and from sparse to dense. The porous-filled crown model exhibits the highest values, while the bare trunk model shows the lowest, and the magnitude of C_L remains small with little difference among the models. This indicates that crown morphology is the dominant factor controlling the mean aerodynamic loading of the tree. A lower crown porosity results in a stronger flow-blocking effect, leading to larger along-wind aerodynamic forces and base bending moments. Further analysis of the drag contribution reveals that the crown accounts for 85%–90% of the total drag and total moment, while the contribution of the trunk to the overall aerodynamic load is relatively limited.

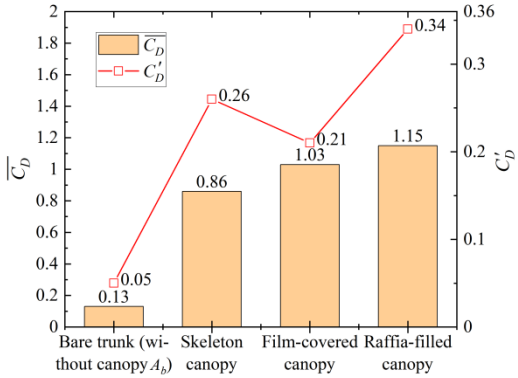

(a) Mean and fluctuating drag coefficient

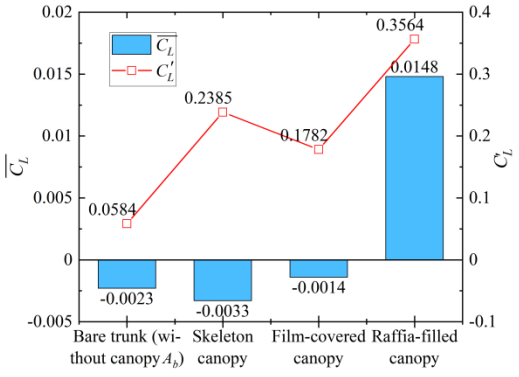

(b) Mean and fluctuating lift coefficient

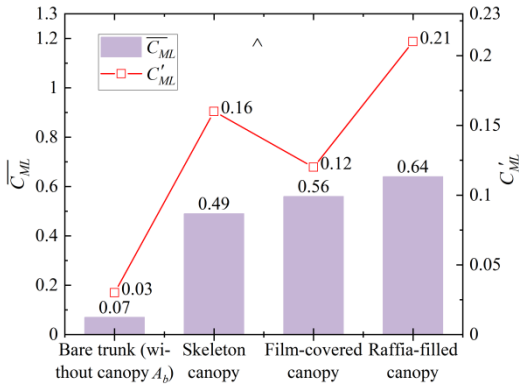

(c) Mean and fluctuating moment coefficient

Figure 4 Mean and fluctuating aerodynamic force coefficients of the tree wind tunnel models

Figure 5 shows the power spectral density (PSD) curves of the drag coefficient C_D, lift coefficient C_L, and moment coefficient C_{ML} for the four tree models, with the corresponding peak frequencies summarized in Table 5. For the bare trunk model, the spectral peak frequencies of C_D, C_L, and C_{ML} are 39.209 Hz, 37.691 Hz, and 39.307 Hz, respectively. These three values are close to each other, reflecting a relatively strong single-frequency dominance in vortex shedding from the bare trunk. It should be noted that because the tree model has a relatively large mass, the aerodynamic force signals acquired by the high-frequency force balance may contain not only the fluctuating components induced by the inflow excitation, but also contributions from the structural dynamic response of the model. Finite element modal analysis of the bare trunk model yields a first-order natural frequency of 42.4 Hz, which is close to the C_D PSD peak in Figure 3-2, suggesting that this peak may be influenced by both the flow fluctuation characteristics and the first-mode response of the model itself. After the crown is introduced, the spectral peak frequencies of all models decrease significantly (by about 40%–55%), and differences exist among different crown configurations. Among them, the porous-filled crown model exhibits the lowest C_D spectral peak frequency.

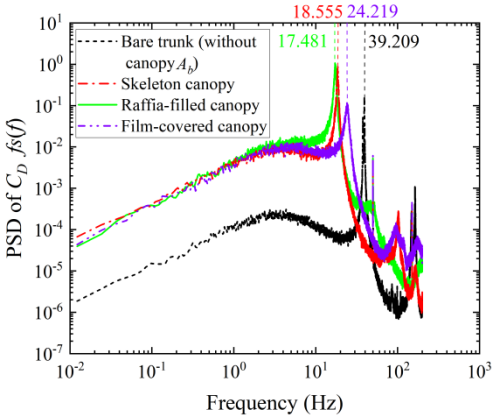

(a) Power spectral density (PSD) of the drag coefficient

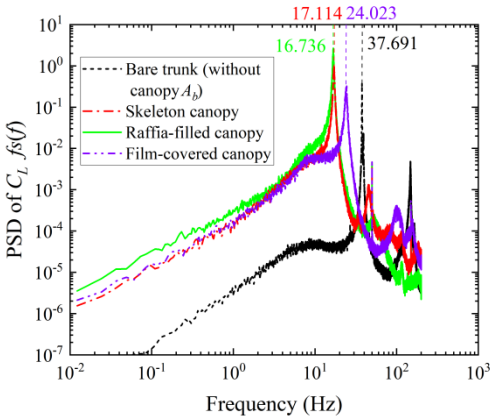

(b) Power spectral density (PSD) of the lift coefficient

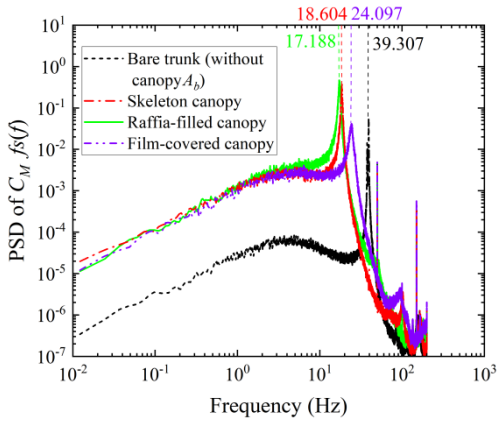

(c) Power spectral density (PSD) of the moment coefficient

Figure 5 Power spectral density (PSD) of aerodynamic force coefficients of tree models

Table 5 Peak frequencies of the power spectral density (PSD) of aerodynamic force coefficients for the tree models

	Bare trunk (without crown)	Skeleton canopy	Film-covered canopy	Raffia-filled canopy
C_D peak frequency	39.209	18.555	24.219	17.481
C_L peak frequency	37.691	17.114	16.736	24.023
C_{ML} peak frequency	39.307	18.604	24.097	17.188

3.2 Wind Loading and Wind-Induced Response from FSI Simulation

To validate the reliability of the FSI solver, the classical FSI benchmark case proposed by Turek and Hron was selected for quantitative verification. In a two-dimensional incompressible laminar channel, a flexible elastic splitter plate is attached to the rear of a rigid cylinder. Under sustained fluid action, the plate undergoes self-excited periodic oscillation and forms a two-way coupling with the wake vortex shedding. Figure 6(a) and (b) compare the displacements in the x and y-directions at the tail of the splitter plate with the results of the Hron–Turek FSI case, while Figure 6(c) and (d) show the flow field and displacement distribution around the model. The displacement characteristics and the flow field structures agree well with those reported by Turek and Hron (2006), confirming the reliability of the FSI solver employed in this study.

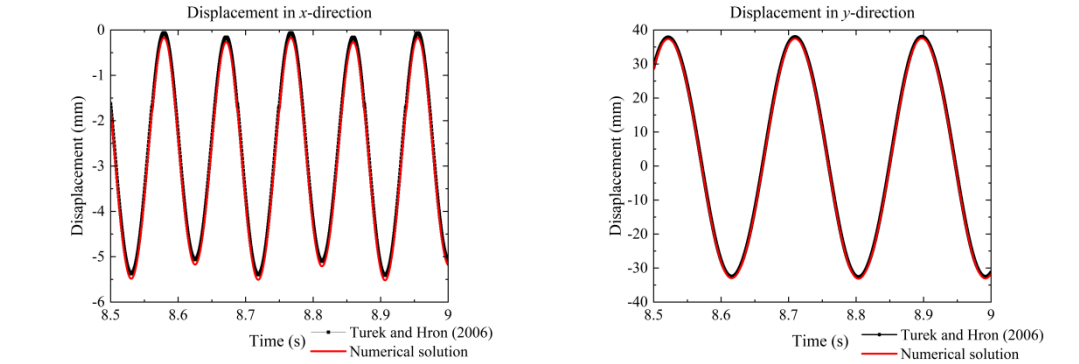

(a) Displacement comparison in *x*-direction (b) Displacement comparison in *y* direction

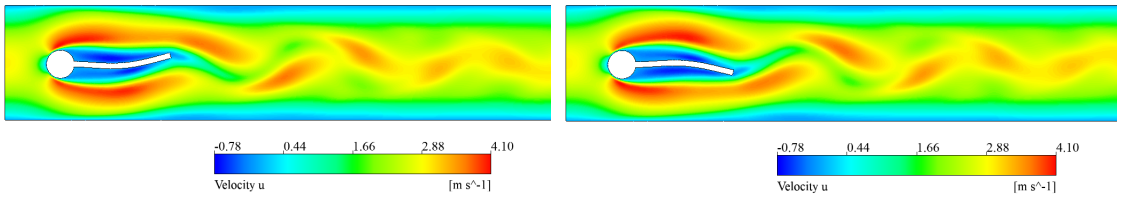

(c) Displacement and velocity regimes

Figure 6 Validation of the FSI Solver with the benchmark case of Turek and Hron

Although the overall deformation amplitude of the tree is relatively limited and does not cause a significant topological restructuring of the large-scale wake, the structural feedback still exerts an influence on the local flow field. Figure 7 shows the instantaneous wake pattern at t=0.6 s under the two-way coupling condition. The streamwise distributions of the normalized mean wind speed and turbulent kinetic energy along the centerline (y/D=0，z/H=0.4) (Figure 8) indicate that the characteristic position in the trunk region under two-way coupling is slightly shifted compared with the one-way coupling case, suggesting that although the wind-induced deformation of the tree is small in magnitude, it is sufficient to alter the local flow boundary conditions. A comparison of the near-wake region downstream of the trunk reveals that the normalized wind speed from the two-way coupling simulation is lower than that from the one-way coupling, and the normalized turbulent kinetic energy peak is also reduced.

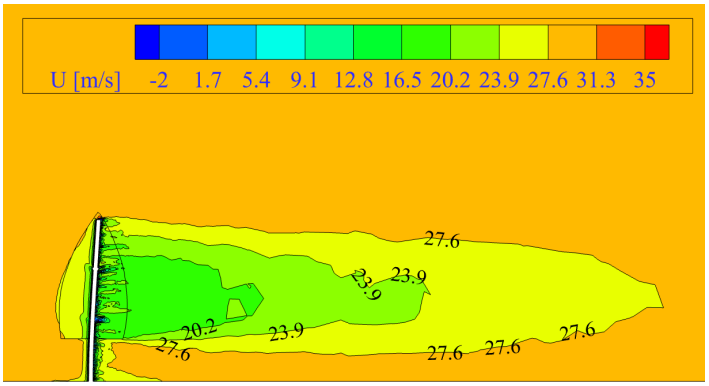

Figure 7 Velocity contour of the tree model at the y=0 plane (t=0.6s)

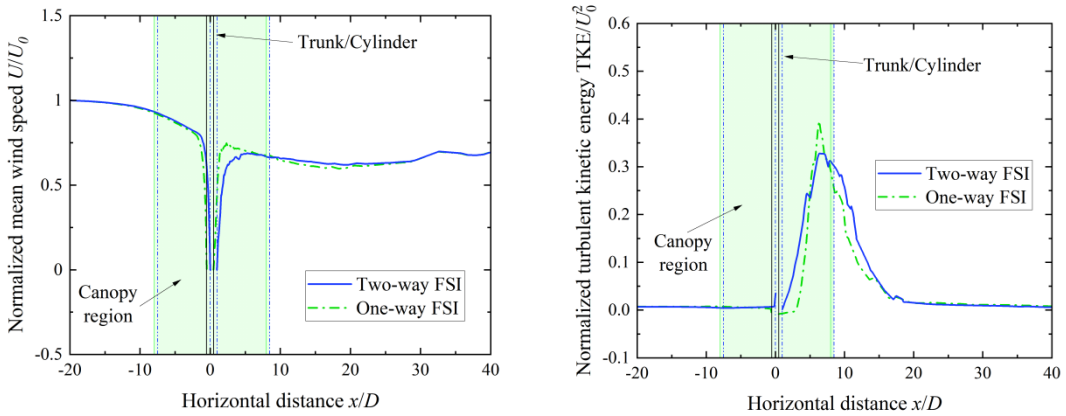

(a) Normalized wind speed (b) Turbulent kinetic energy

Figure 8 Normalized wind speed and turbulent kinetic energy along the centerline (y/D=0, z/H=0.4) of the tree model

A velocity monitoring point B was set at a distance of 2 m downstream from the center of the trunk base and at a height of 0.8 m to record the along-wind velocity time history. As shown in Figure 9, the wind speed at the monitoring point fluctuates with time under both one-way and two-way coupling conditions. However, the fluctuation amplitude under two-way coupling is significantly larger than that under one-way coupling, with more frequent peak-valley variations, reflecting a stronger turbulent fluctuation character.

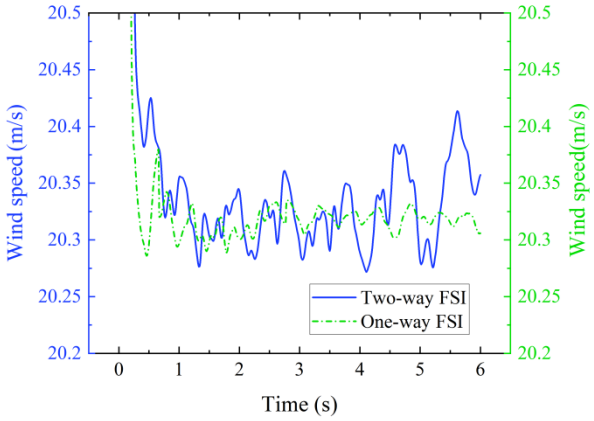

Figure 9 Comparison of wind velocity time histories at monitoring point B (2, 0, 0.8) downstream of the tree

As shown in Table 6 and Figure 10, the aerodynamic force response of the tree model under two-way FSI coupling is more pronounced than under one-way coupling. The statistical results indicate that two-way coupling slightly reduces the mean drag, whereas the fluctuating drag, mean lift, and fluctuating lift all increase, with the fluctuating lift showing the most significant increase. Spectral analysis further reveals that under two-way coupling the fluctuating lift energy is distributed over a wider frequency range, the band around the main peak broadens, and the energy at medium and high frequencies is enhanced.

Table 6 Comparison of mean and fluctuating aerodynamic forces of the tree model (Unit: N)

Simulation method	Mean drag $\overline{F}_D$	Fluctuating drag F'_D	Mean lift $\overline{F}_L$	Fluctuating lift F'_L
Two-way FSI	266.51	0.78	0.47	1.45
One-way FSI	267.67	0.52	0.43	1.07

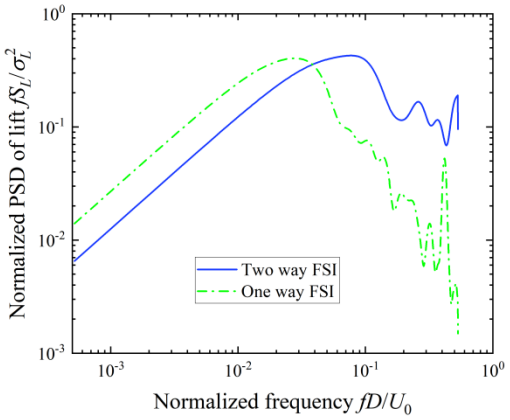

Figure 10 Comparison of aerodynamic force spectra for the tree

Table 7 presents the statistical results of the displacement response at the top of the tree trunk under two-way and one-way FSI coupling. Under two-way coupling, the mean along-wind displacement is slightly lower than under one-way coupling, whereas the maximum along-wind displacement and both the mean and maximum cross-wind displacements increase markedly. This indicates that two-way FSI coupling weakens the mean along-wind loading on the tree to some extent, but enhances the excitation effect of flow disturbances on the structure, making the fluctuating and extreme responses at the tree top more significant.

Table 7 Mean, fluctuating, and maximum displacements at the top of the tree model trunk (Unit: mm)

Simulation method	Mean displacement		Fluctuating displacement		Maximum displacement	
	Along-wind $\overline{D}_x$	Cross-wind $\overline{D}_y$	Along-wind D'_x	Cross-wind D'_y	Along-wind $D_{x,\max}$	Cross-wind $D_{y,\max}$
Two-way FSI	58.64	3.42	1.62	0.96	62.75	4.77
One-way FSI	58.91	2.89	1.18	0.71	60.80	4.26

In terms of deformation modes, the key frames of the along-wind and cross-wind deformations shown in Figure 11 and Figure 12 reveal distinct response characteristics in the two directions. Along-wind deformation is dominated by aerostatic deflection, with the displacement time history characterized by small-amplitude oscillations around a shifted

mean position. In contrast, cross-wind deformation mainly features periodic swaying driven by dynamic vibration.

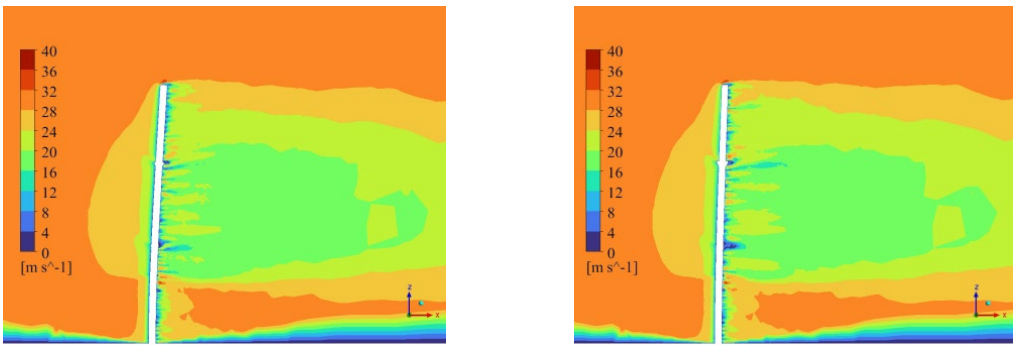

（a）t=0.6s　　（b）t=4s

Figure 11 Key Frames of Along-Wind Deformation of the Tree Model

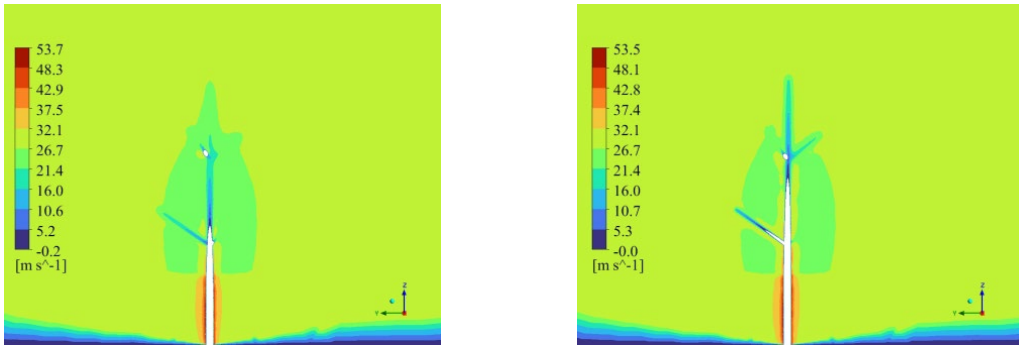

（a）t=0.6s　　（b）t=4s

Figure 12 Key Frames of Cross-Wind Deformation of the Tree Model

Figure 13 (a) shows the along-wind displacement time histories at the tree top under the two coupling cases, and Figure 13 (b) presents the corresponding normalized power spectral densities. Under two-way coupling, the displacement oscillation amplitude is generally larger than under one-way coupling, with a more pronounced waveform fluctuation; the one-way coupled response is relatively stable with a smaller vibration amplitude. Spectral results indicate that the displacement spectral peak is higher under two-way coupling (peak value 1.27), but the peak shape is significantly broader than that under one-way coupling (peak value 0.75), with energy distributed over a wider frequency band. Because the one-way coupling does not consider the effect of structural motion on the flow field, the aerodynamic excitation frequency components are relatively concentrated, resulting in a sharper structural response spectral peak.

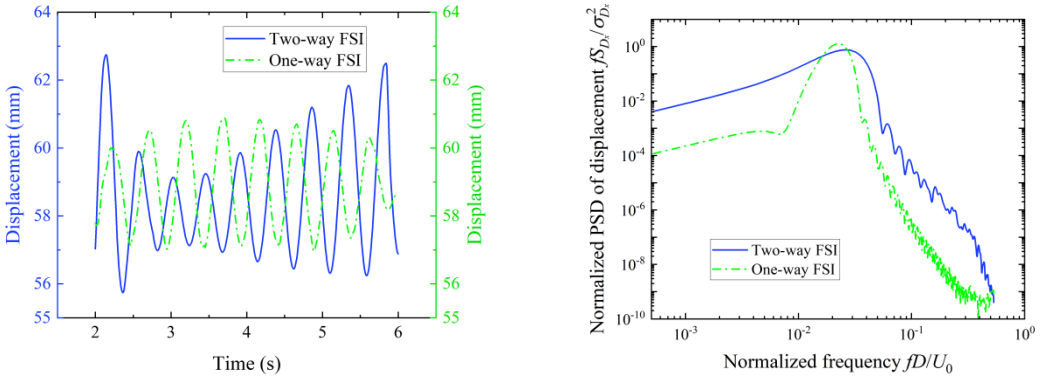

(a) Time histories (b) Normalized power spectral density

Figure 13 Along-wind displacement response at the tree top under one-way and two-way FSI coupling

5. Research Group

(1). Jingxuewang (Representative Researcher)

(2). Collaborate Researchers

Akihito Yoshida

Zhongcan Chen

Qingshan Yang

Yukio Tamura

Haiyang Wang

6. Abstract (half page)

Research Theme: Aerodynamic characteristics of a tree model based on wind tunnel test and FSI simulation

Representative Researcher (Affiliation): Jingxue Wang

Summary · Figures

Wind-induced tree failure poses a significant risk in urban and forest environments. Understanding how crown characteristics influence wind-induced effect of trees is essential for prediction of tree failure under strong wind conditions. This study systematically investigates the influence of crown morphology on the aerodynamic characteristics and wind-induced responses of trees through wind tunnel tests, and fluid–structure interaction (FSI) simulations. Results of high-frequency force balance test show that the along-wind force coefficient and the base moment coefficient are the dominant aerodynamic load components, both increasing monotonically as the crown changes from sparse to dense. The crown accounts for 85%–90% of the total mean drag and moment, making it the primary factor governing the aerodynamic loading. The introduction of a crown reduces the spectral peak frequencies of the drag, lift, and moment coefficients by about 40%–55% relative to the bare trunk model, with the porous-filled crown model exhibiting the lowest drag coefficient peak frequency among the crowned models. Through two-way FSI simulation, the normalized mean wind speed and turbulent kinetic energy peak along the wake centerline are lower than those under one-way coupling, while the along-wind velocity fluctuation amplitude at the downstream monitoring point increases. Two-way coupling slightly reduces the mean drag but enhances the fluctuating drag, mean lift, and fluctuating lift, with the aerodynamic force spectra showing a broadened energy distribution and stronger medium-and-high-frequency content. In terms of displacement, two-way coupling leads to amplified fluctuating and peak responses in both directions, despite a marginal reduction in the mean along-wind displacement. The corresponding displacement spectra reveal a wider and less concentrated energy distribution.